J Sol-Gel Sci Technol
DOI 10.1007/s10971-017-4554-1

ORIGINAL PAPER: SOL-GEL AND HYBRID MATERIALS FOR CATALYTIC, PHOTOELECTROCHEMICAL AND SENSOR APPLICATIONS

Black ZnO/C nanocomposite photocatalytic films formed by one-step sol–gel technique

N. M. Denisov[1] · E. B. Chubenko[1] · V. P. Bondarenko[1] · V. E. Borisenko[1]

Received: 2 September 2017 / Accepted: 23 November 2017

Abstract We developed a facile one-step sol–gel technique for fabrication of black zinc oxide/carbon (ZnO/C) nanocomposite films demonstrating an enhanced photocatalytic activity. Amorphous carbon covering ZnO grains inside the films was reduced from organic components of the zinc acetate based sol calcinated at 500 °C. The amount of carbon in the films can be controlled by varying the amount of zinc chloride added to the zinc acetate based sols. The surface layer of the films is composed by randomly oriented hexagon-shaped ZnO grains. Photoluminescence quenching indicating the suppression of electron-hole recombination in the prepared ZnO/C composites were observed. The recorded optical transmittance/reflectance spectra and the performed photocatalytic tests demonstrated that the synthesized ZnO/C nanocomposite is promising for photoinduced decomposition of organic compounds. Related peculiarities are discussed.

Graphical abstract

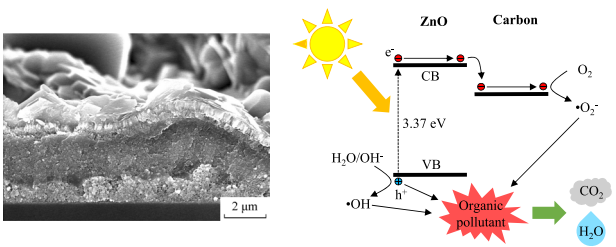

✉ N. M. Denisov
waefae@gmail.com

[1] Department of Micro- and Nanoelectronics, Belarusian State University of Informatics and Radioelectronics, P. Browka 6, 220013 Minsk, Belarus

Keywords ZnO/C · Nanocomposite · Sol–gel · Photocatalysis

1 Introduction

Hazardous wastes of industrial, agricultural, and domestic activities are becoming one of the major ecological challenges, threatening the aquatic ecosystems and the drinking water quality. Moreover, conventional water purification technologies are ineffective against persistent organic pollutants, which spread out rapidly in air and water [1]. They can be destroyed or neutralized by using advanced oxidation processes [2]. Heterogeneous photocatalysis, being one of these processes, has demonstrated its efficiency in degrading a wide range of organic pollutants [3]. This method utilizes an ability of semiconductor materials to generate electron-hole pairs upon absorption of solar light, which in turn produce highly reactive •OH and $•O_2^-$ radicals in water and humid air. The photogenerated charge carriers along with the produced radicals provide effective decomposition of organic compounds into carbon dioxide and water [4].

Zinc oxide (ZnO) is one of the most widely used photocatalytic materials due to its low cost, non-toxicity, and high photocatalytic activity [5]. ZnO films can be fabricated by numerous deposition techniques: chemical, hydrothermal, electrochemical, and sol–gel. However, because of the wide band gap (3.37 eV [6]) it can only absorb ultraviolet (UV) radiation, which is about 3–4% of the solar light reaching the terrestrial surface [7]. ZnO is also known to be prone to photocorrosion caused by photogenerated holes, which has been found to decrease its photocatalytic activity

Published online: 29 November 2017

in time [8]. In order to overcome the above limitations ZnO should be combined with other materials to form heterostructures or hybrid materials with an improved visible light absorption and charge carrier separation [9].

Among possible candidates for integration with ZnO, there are carbon materials, which are characterized by a low cost, non-toxicity [10], and a potential for an improvement of photocatalytic properties of the composition in a variety of ways [11]. Depending on the structural form of carbon (i.e., nanotubes, graphene, nanodots, fibers, spheres, or activated carbon) carbon atoms were reported to act as photoelectron scavengers, photosensitizers, and co-adsorbents during photocatalytic processes. These roles have been observed in the improved photocatalytic activity under UV and visible light irradiation, as well as in the photocorrosion stability and reusability of ZnO/carbon (ZnO/C) composites.

There are two principal approaches to fabrication of ZnO/C composites. One of them supposes a use of preliminarily formed carbonaceous substrates [12, 13] or nanocarbon additives (nanotubes, fullerenes, graphene flakes, nanoparticles) in the synthesis of ZnO from precursor solutions [14–18]. The second one involves reduction of carbon from accompanying organic compounds during thermal processing of ZnO precursors [19, 20]. It facilitates mixing of ZnO and carbon in the composite film providing tight electronic interaction between components during photocatalytic processes. Thus, new approaches to fabrication of ZnO/C composites are of practical importance.

In this paper, we report a zinc chloride ($ZnCl_2$) mediated formation of black ZnO/C nanocomposite films through a conventional one-step sol–gel deposition process. We supposed a priori and then experimentally confirmed that it could provide synthesis of ZnO/C nanocomposites within one calcination step. Structure, composition, optical and photocatalytic properties of the composite films are presented and discussed.

2 Materials and methods

Microscope glass slides as thick as 1 mm were used as substrates. They were cut into 2.0×2.5 cm^2 pieces, cleaned in acetone and distilled water, and then dried in air.

Two types of sols were composed to fabricate ZnO-containing films on the glass substrates. The first, which is the basic one, consisted of a mixture of isopropyl alcohol (C_3H_7OH), monoethanolamine (NH_2–CH_2CH_2–OH) and anhydrous zinc acetate ($(CH_3COO)_2Zn$) with their molar ratio of 49:7:5, respectively. The second one was prepared by adding 1.15–8.05 wt.% of $ZnCl_2$ into the basic sol. Both sols were aged for 2 days at room temperature.

There were two groups of samples with ZnO-containing films. In both groups the film fabrication started with immersion of the glass substrates into the basic sol for 1 min followed by their slow withdrawal and drying at 200 °C for 5 min in air. This procedure was repeated 4 times in order to achieve an appropriate thickness of the deposited films. Then the samples were annealed in air at 500 °C for 30 min. It was the final processing step for the first group of the samples, which are considered to be reference samples. The second group included the samples processed like the ones of the first group, but with additional films deposited by fourfold immersion/drying with the use of the $ZnCl_2$ containing sol, and finalized by annealing in the regime of the first group of the samples.

The surface morphology of the films was analyzed by scanning electron microscopy (SEM) with Hitachi S-4800. Their elemental composition was determined by energy-dispersive X-ray spectroscopy (EDX) with Bruker QUANTAX 200. Optical reflectance/transmittance spectra of the samples were recorded with Proscan MC-121 UV-VIS-NIR spectrophotometer in the wavelength range of 300–1000 nm at room temperature. Photoluminescence (PL) spectra were registered at room temperature with a spectroscopic complex based on Solar TII MS 7504i spectrograph equipped with the Peltier cooled back-thinned silicon FFT-CCD detector (Hamamatsu S7031-1006S). The luminescence of the samples was excited by the light of 1 kW xenon lamp at the wavelength of 345 nm cut from the broad emission spectrum by double monochromator Solar TII DM 160. We also registered Raman spectra with SOL Instruments Confotec NR500 scanning laser confocal Raman microscope using 473 nm Cobolt Blues 25 DPSS laser as a light source. All optical measurements were carried out at room temperature.

Special attention was given to photocatalytic activity of the fabricated films. It was evaluated by degradation of the organic dye Rhodamine B (RhB) under ultraviolet (UV) light irradiation in the presence of the films. Each sample was immersed into 3 ml of 10 mg/l RhB water solution, which was being continuously stirred by a laboratory shaker at 180 r.p.m. Prior to the UV exposure each sample was kept in the solution in dark for 30 min to reach an adsorption/desorption equilibrium of the dye at the surface of the film. During the photocatalytic activity tests the solutions were placed 2 cm far from an 8 W mercury discharge lamp equipped with a 365 nm light filter. Optical absorption spectra of a 2 ml probe taken from the RhB solutions were recorded upon every 15 min of irradiation using Proscan MC 121 spectrophotometer. The concentration of RhB left in the solutions was calculated from the intensity of their absorption at the wavelength of 556 nm (peak at the spectrum of RhB) using the preliminarily taken calibration

curve. After the test the probe was returned into the solution.

3 Results

Impressive visual difference between the films fabricated from the sols without $ZnCl_2$ (group I) and with $ZnCl_2$ (group II) was noticed immediately upon calcination at 500 °C. It is illustrated in Fig. 1. The reference group I samples were matt white, which is typical for a pure ZnO film on a transparent substrate. The group II samples were black from the film side. The presence of carbon that is responsible for this coloration, was revealed by subsequent analysis of the surface morphology, content of chemical elements, and Raman data. The experimental arguments are as follows.

Figure 2 presents surface images of the films from the two groups. There is a dramatic difference in their surface morphology, while all of them have a rough texture. The surface of the films fabricated from the basic sol (without $ZnCl_2$) is formed by few micrometer sized agglomerates of submicron (50–150 nm) grains. In contrast, randomly oriented hexagon-like structures of few micrometers in size are well resolved at the surface of the black films derived from the $ZnCl_2$ containing sol, which is not surprising, noting that the most thermodynamically stable wurtzite crystalline phase of ZnO has a hexagonal crystal lattice [9].

Cross-sectional SEM images of the experimental black films and reference white films show their thickness to vary in the range of 2–6 μm due to the roughness. The reference films are uniform in a cross-section and consist of sub-micron grains also visible at their surfaces. The black films have a three-layer structure illustrated in Fig. 3. The surface layer is composed by the hexagonal grains. As far as they do not penetrate inside the film, one can assume them to originate from the liquid $ZnCl_2$ melted during the second annealing at 500 °C and subsequent crystallization of ZnO from the melted phase.

Two entire regions with slightly different electronic contrast are observed under the grains. Both of them are

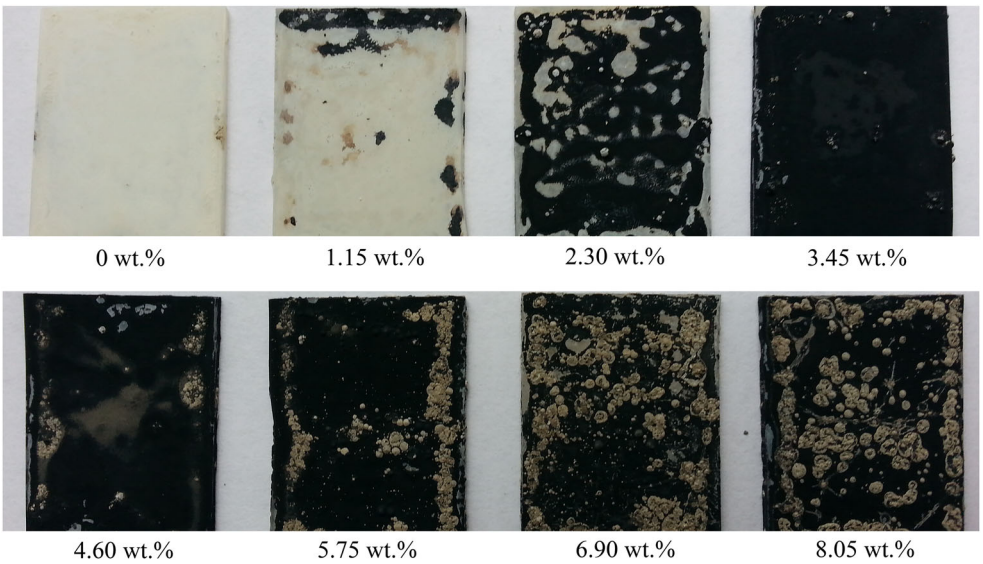

Fig. 1 Surface view of the samples with ZnO (0 wt.% $ZnCl_2$) and ZnO/C (1.15–8.05 wt.% $ZnCl_2$) films

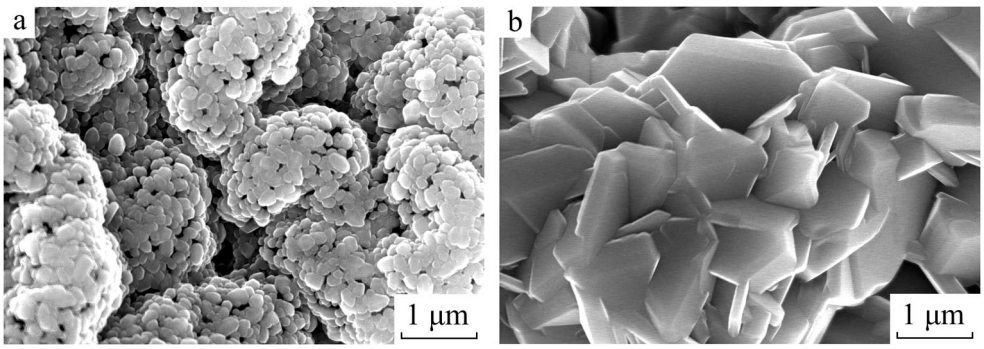

Fig. 2 SEM surface images of the films fabricated from the basic sol (**a**) and the sol with 4.6 wt.% of $ZnCl_2$ (**b**)

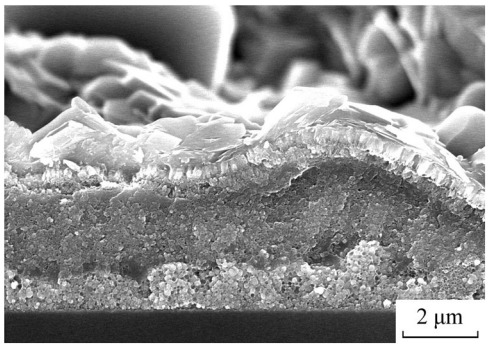

Fig. 3 SEM image of the cross-section of the black film fabricated from the sol with 4.6 wt.% of $ZnCl_2$

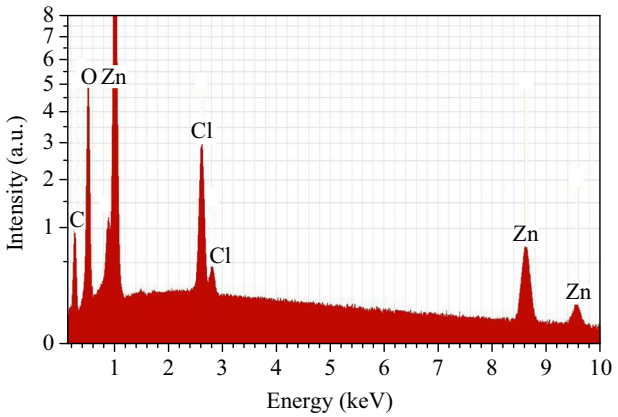

Fig. 4 EDX spectrum of the black film fabricated from the sol with 4.6 wt.% of $ZnCl_2$

formed by submicron grains, while the grains in the near-substrate region are in average and a little bit larger in size. It looks quite reasonable, since the bottom layer of the black films was twice subjected to the annealing at 500 °C, which inevitably initiated the growth of the grains. Considering the transparency of ZnO in the visible range also confirmed by the white color of the reference samples, we conclude that the black pigment in the films derived from the $ZnCl_2$ containing sol is localized in the intermediate layer, which looks the darkest in Fig. 3. As far as no visible precipitates are resolved in it, one can suppose this pigment to be uniformly dispersed in this layer.

The EDX analysis of the black films found carbon in concentrations above the level registered in the reference sample, in which this element belonged to the products of the organic components of the sol and organic compounds adsorbed at the surface after the film formation. The recorded EDX spectrum is presented in Fig. 4. Carbon concentration in the black films was estimated to be about 5 wt.%. It seems to be sufficient for coloration of the film, although it should be taken into account that EDX detects carbon atoms only in the near-surface layer of the film (not

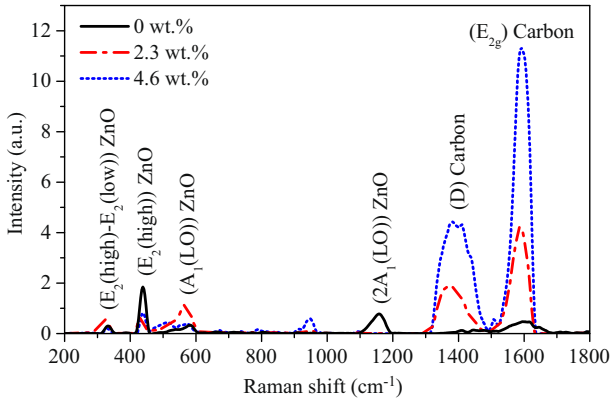

Fig. 5 Raman spectra of the ZnO reference and black films fabricated from the sols with 2.3 wt.% and 4.6 wt.% of $ZnCl_2$ (excitation wavelength 473 nm)

deeper than 1–2 μm). The $ZnCl_2$-containing precursor also leaves a fingerprint in the EDX spectrum in the form of the well-distinguishable signals from chlorine (Cl) left in the black films. Its concentration and carbon concentration in the films correlate with the amount of $ZnCl_2$ added to the sol.

Typical carbon related signals were also detected by Raman spectrometry. The Raman spectra recorded for the black film and reference samples are shown in Fig. 5. There are two groups of peaks in the Raman spectra related to ZnO and carbon in the analyzed films. The peaks located at 333, 438, 574, and 1158 cm^{-1} correspond to E_2(high)-E_2(low), E_2(high), A_1(LO), $2A_1$(LO) vibrational modes of crystalline ZnO bonds [21], respectively. Another two pronounced typical peaks at 1380 and 1588 cm^{-1} are usually attributed to structural disorder (designated as "D") and E_{2g} vibrational mode of C–C sp^2 bonds in carbon [22]. Note that these carbon-related peaks were also registered in the ZnO reference film but at a dramatically lower intensity as compared to the black films. That agrees with the results of the EDX analysis. Characteristic signals from $ZnCl_2$ at around 250 cm^{-1} [23] were not detected.

Summarizing the experimental observations presented, we conclude that the addition of $ZnCl_2$ into the sol used for the sol–gel fabrication of the films results in the formation of ZnO/C nanocomposite. Amorphous carbon is quasi-uniformly dispersed between the ZnO grains in the intermediate layer thus giving rise to the black color of the films.

Room temperature PL spectra of the reference and black samples are compared in Fig. 6. Several bands are resolved. The narrow PL band peaking at 375 nm corresponds to the radiative band-to-band recombination processes in crystalline ZnO [15, 17, 24]. This wavelength corresponds to the energy of 3.31 eV. Considering the exciton-binding energy of 60 meV in ZnO [25], the fundamental band gap in both samples is estimated to be of 3.37 eV. The PL band with the

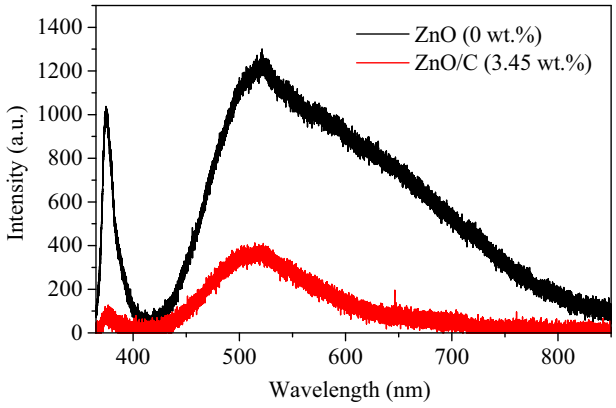

Fig. 6 Room temperature PL spectra for the reference ZnO film and black ZnO/C film fabricated from the sol with 3.45 wt.% of $ZnCl_2$

maximum at 520 nm is usually attributed to recombination processes via energy levels in the ZnO band gap associated with oxygen vacancies [26, 27]. Broadening of this band into infrared spectral region is more probably controlled by interstitial oxygen atoms which energy states are responsible for the luminescence in the range of 550–800 nm [26–28].

While the energy positions of the main PL peaks are practically identical for both samples, the reference one demonstrates more intense photoluminescence. Such PL quenching is often reported for carbon-containing ZnO structures [13–17, 19, 24]. It is usually attributed to the photoelectron scavenging by carbon materials leading to the suppression of electron-hole recombination in ZnO.

Optical transmittance and reflectance of the reference and black samples were measured as a preliminary step assessment of their suitability for an efficient photocatalysis. The recorded spectra are presented in Fig. 7. Note that the glass substrates used are 86–90% transparent in the wavelength range of 356–1000 nm, but their transparency drops from 86 to 4% with decreasing the wavelength from 356 to 300 nm. The spectra of the reference film look typical for ZnO films. Its transmittance gradually changes from about 4% to less than 0.4% for the wavelengths decreasing from 1000 to 400 nm. The reflectance in this wave range varies slightly between 0.4 and 1.3%. Both spectra are characterized by drop of the signal intensities almost to zero in the UV range below 400 nm.

The optical band gap of ZnO extracted from these parts of the spectra is 3.15 eV, which agrees well with the published data (3.08–3.44 eV [29]), although such low value can be related to the contribution of donor defects to the light absorption suggested in ref. [30]. In contrast to the reference samples, the black ones are characterized by wavelength-independent transmittance and reflectance being close to 0 %.

The significant difference in the optical characteristics of the reference and black films was developed in the

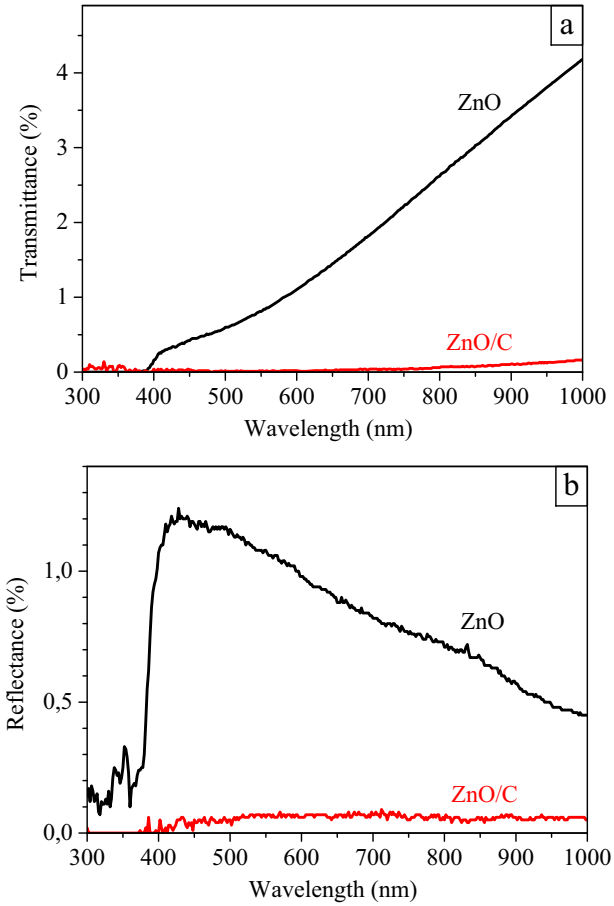

Fig. 7 Transmittance (**a**) and reflectance (**b**) spectra of the ZnO reference and black ZnO/C films fabricated from the sol with 3.45 wt. % of $ZnCl_2$

performed photocatalytic tests. Figure 8 shows the adsorption and photocatalytic degradation of RhB in water solution irradiated by UV light with reference and black films in terms of the decrease of its concentration ratio C/C_0, where C_0 and C are starting and resulting concentrations of RhB, respectively. Accounting for the high photocatalytic activity of the tested samples they were kept for 30 min in the solution in dark, before irradiation by UV light in order to stabilize adsorption processes at their surfaces. Upon 60 min of UV irradiation all tested catalysts decolorized the RhB solutions completely. Nevertheless, the reference ZnO film demonstrated the lowest adsorption capacity and photocatalytic activity. At the same time, the most uniformly black ZnO/C film derived from the sol containing 3.45 wt.% of $ZnCl_2$ adsorbed 6.9 times more RhB, showing the highest adsorption capacity, while the highest photocatalytic degradation rate (16.5% higher than for the reference ZnO film) was demonstrated by the film fabricated from the sol containing 6.90 wt.% of $ZnCl_2$, which apparently adsorbed only 2.75 times more RhB than the reference ZnO film.

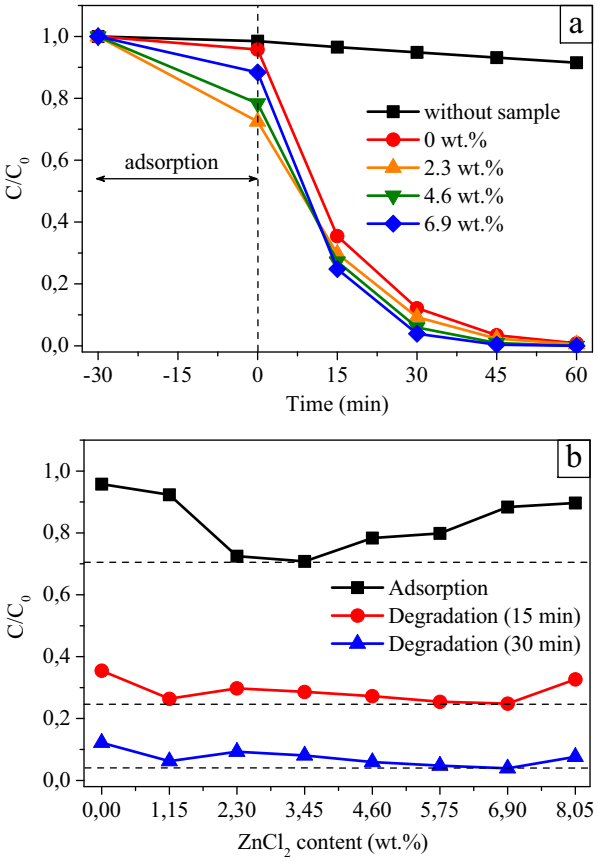

Fig. 8 Adsorption and photocatalytic degradation of RhB in the water solution by ZnO reference and black ZnO/C films under UV light (365 nm) irradiation: **a**–depending on the time for various concentrations of $ZnCl_2$ in the initial sols; **b**–depending on the concentration of $ZnCl_2$ in the initial sols for various times

4 Discussion

Analyzing the sources of carbon in the sol–gel derived ZnO films, one should first take into consideration the organic components of the sol, which are isopropyl alcohol (boiling at 82.6 °C), monoethanolamine (boiling at 170 °C), and anhydrous zinc acetate (decomposing at 237 °C). The first two liquid components are expected to evaporate during drying of the films at 200 °C. Therefore, we consider zinc acetate to be the main source of carbon in the resulting ZnO/C nanocomposites. Zinc acetate, as follows from [31, 32], decomposes at 150–300 °C producing acetic acid, acetone, CO_2, and ZnO nanoparticles. It is known [33] that such particles can be covered with acetyl groups, unless oxygen flow conditions are applied during the thermal treatment [34]. In case zinc acetate is heated in air, the final combustion of organic by-products occurs at 370–490 °C [31]. However, a fraction of carbon containing species can remain in closed pockets and pores of the ZnO agglomerates, which are of several microns in size. Carbon atoms do not enter the crystalline lattice and dope ZnO, as it is

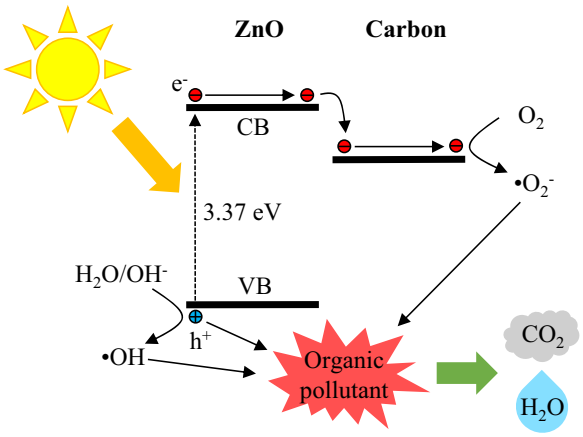

Fig. 9 A mechanism of photocatalytic degradation of Rhodamine B by ZnO/C nanocomposites

evident from the experimentally extracted optical band gap in the reference samples corresponding to that of bulk ZnO crystals. The addition of $ZnCl_2$ to the sol dramatically modifies carbon-involved processes. This compound is known to be a moderate-strength Lewis acid capable of catalyzing synthesis and decomposition of different hydrocarbons [35], including the decomposition of organic substances into carbon [36–38]. These reactions usually take place in the melted $ZnCl_2$ media. Its melting point is 290 °C. While all carbon-containing compounds used in our experiments have lower boiling or decomposition temperature, their vapors and decomposition products can be adsorbed at the surfaces of the forming ZnO grains and trapped inside their agglomerates. Then they undergo pyrolysis in the presence of melted $ZnCl_2$ catalyst resulting in the formation of amorphous carbon. The produced carbon is blocked inside the intermediate layer by the melted $ZnCl_2$, which in turn reacts with oxygen producing the ZnO layer at the surface. This dense layer hinders an access of oxygen to the underlying melted $ZnCl_2$, which is supported by the observation of the Cl-related peaks at the EDX spectra.

The mechanism of the photocatalytic degradation of Rhodamine B by ZnO/C nanocomposites previously proposed by various researchers [12, 13, 16–18] is shown in Fig. 9. First, absorption of UV light in the material excites electrons from the valence band of ZnO to move to the conduction band, thus producing electron-hole pairs. These pairs can either recombine or take part in photocatalytic reactions. Next, the route of the photocatalytic reactions is determined by the presence of adsorbed species and heterojunctions at the surface of ZnO. When an electron-hole pairs migrate to the ZnO/C heterojunctions, the electrons can be transferred to the carbon particles preventing recombination of the photogenerated charge carriers and improving the efficiency of irradiation energy utilization. When charge carriers migrate to the ZnO/water or carbon/

water interface, they interact with the species adsorbed from the water. Holes can either directly oxidize the adsorbed RhB or produce hydroxyl radicals (•OH) from water molecules (H_2O) or hydroxide ions (OH^-). Electrons can turn oxygen molecules (O_2) into superoxide radicals ($•O_2^-$), which can further react with H_2O to produce •OH radicals, hydroperoxyl radicals ($HO_2•$), and hydrogen peroxide (H_2O_2). Finally, the produced radicals react with RhB and decompose it into more simple organic compounds, which are further degraded by newly generated charge carriers and radicals into water and carbon dioxide.

The increased adsorption capacity of the black films can be attributed to the presence of carbon facilitating the adsorption of organic molecules, as it was reported in [11, 12, 24], and allowing their direct oxidation by photogenerated holes [20]. However, the adsorption capacity of the ZnO/C composite films does not seem to correlate with their photocatalytic activity. As it is shown in ref. [15], the efficiency of ZnO/C photocatalysts is related not only to their surface area, but also to the nature of the carbon material.

As for the photocatalytic role of carbon, its species were reported in refs. [10–17, 19, 24] to be able to act as photoelectron reservoirs providing a necessary separation of photogenerated electrons and holes, which results in the reduction of recombination losses and improvement of the photocatalytic activity of ZnO. The most active ZnO/C films derived from the sol containing 6.90 wt.% of $ZnCl_2$ showed 16.5% higher RhB degradation rate than the reference ZnO film. It can be explained by the surface states at ZnO grains providing good electrical contact between the grains and carbon material via C–O–Zn bonds discussed in refs. [11, 12, 14, 24]. An enhanced light absorption by the intergrain carbon material seems to be an additional factor increasing the photocatalytic activity of the sol–gel fabricated ZnO/C composites.

5 Conclusion

The proposed addition of $ZnCl_2$ into the sol for sol–gel fabrication of ZnO based films allows one calcination step at 500 °C to be sufficient for the formation of black ZnO/C nanocomposites with an enhanced photocatalytic activity as compared with the reference ZnO film. Amorphous carbon filling the regions between the synthesized ZnO nanograins is supposed to be formed as a result of the catalytic effect of the melted $ZnCl_2$ on decomposition of the organic components of the sol. The melt is blocked by the growing hexagon-shaped ZnO crystallites at its surface. The incorporated carbon enhances light absorption and transport of the photogenerated carriers thus increasing the photocatalytic activity of the composite.

Acknowledgements This work was supported through the Project 3.2.04 of the National Program "Convergence" (Belarus) and Project 2.1.02 of the Belarus Government Research Program "Photonics, Optoelectronics, and Microelectronics". The authors are grateful to D. V. Zhigulin for the SEM and EDX analysis of the samples.

Compliance with ethical standards

Conflict of interest The authors declare that they have no competing interests.

References

1. Mahlambi MM, Ngila CJ, Mamba BB (2015) Recent developments in environmental photocatalytic degradation of organic pollutants: the case of titanium dioxide nanoparticles—a review. J Nanomater. https://doi.org/10.1155/2015/790173
2. Deng Y, Zhao R (2015) Curr Pollut Rep 1:167–176
3. Chong MN, Jin B, Chow CWK, Saint C (2010) Water Res 44:2997–3027
4. Ibhadon AO, Fitzpatrick P (2013) Catalysts 3:189–218
5. Adnan MAM, Julkapli NM, Hamid SBA (2016) Rev Inorg Chem 36:77–104
6. Kołodziejczak-Radzimska A, Jesionowski T (2014) Materials 7:2833–2881
7. Spasiano D, Marotta R, Malato S, Fernandez-Ibanez P, Somma ID (2015) Appl Catal B 170:90–123
8. Lee KM, Lai CW, Ngai KS, Juan JC (2016) Water Res 88:428–448
9. Johar MA, Afzal RA, Alazba AA, Manzoor U (2015) Photocatalysis and bandgap engineering using ZnO nanocomposites. Adv Mater Sci Eng. https://doi.org/10.1155/2015/934587
10. Chen H, Wang L (2014) Beilstein J Nanotechnol 5:696–710
11. Han C, Yang M-Q, Weng B, Xu Y-J (2014) Phys Chem Chem Phys 16:16891–16903
12. Qu J, Luo C, Cong Q (2012) Micro Nano Lett 7:1064–1068
13. Mu J, Shao C, Guo Z, Zhang Z, Zhang M, Zhang P, Chen B, Liu Y (2011) ACS Appl Mater Interfaces 3:590–596
14. Yan Y, Chang T, Wei P, Kang S-Z, Mu J (2009) J Disper Sci Technol 30:198–203
15. Sampaio MJ, Bacsa RR, Benyounes A, Axet R, Serp P, Silva CG, Silva AMT, Faria JL (2015) J Catal 331:172–180
16. Fu L, Lai G, Zhang H, Yu A (2015) J Nanosci Nanotechnol 15:4325–4331
17. Li Y, Zhang B-P, Zhao J-X, Ge Z-H, Zhao X-K, Zou L (2013) Appl Surf Sci 279:367–373
18. Byrappa K, Subramani AK, Ananda S, Lokanatha Rai KM, Sunitha MH, Basavalingu B, Soga K (2006) J Mater Sci 41:1355–1362
19. Yu H-F, Chou H-Y (2013) Powder Technol 233:201–207
20. Zhang L, Cheng H, Zong R, Zhu Y (2009) J Phys Chem C 113:2368–2374
21. Cusco R, Alarcon-Llado E, Ibanez J, Artus L (2007) Temperature dependence of Raman scattering in ZnO. Phys Rev B. https://doi.org/10.1103/PhysRevB.75.165202
22. Wang Y, Alsmeyer DC, McCreery RL (1990) Chem Mater 2:557–563
23. James DW, Parry RM, Leong WH (1978) J Raman Spectrosc 7:71–73
24. Samadi M, Shivaee HA, Pourjavadi A, Moshfegh AZ (2013) Appl Catal A 466:153–160
25. Djurisic AB, Leung YH (2006) Small 2:944–961

26. Tu N, Tuan NT, Dung NV, Cuong ND, Kien NDT, Huy PT, Hieu NV, Nguyen DH (2014) J Lumin 156:199–204
27. Epie EN, Chu WK (2016) Appl Surf Sci 371:28–34
28. Vempati S, Mitra J, Dawson P (2012) One-step synthesis of ZnO nanosheets: a blue-white fluorophore. Nanoscale Res Lett. https://doi.org/10.1186/1556-276X-7-470
29. Arif A, Belahssen O, Gareh S, Benramache S (2015) The calculation of band gap energy in zinc oxide films. J Semicond. https://doi.org/10.1088/1674-4926/36/1/013001
30. Srikant V, Clarke DR (1998) J Appl Phys 83:5447–5451
31. Mihaiu S, Szilágyi IM, Atkinson I, Mocioiu OC, Hunyadi D, Pandele-Cusu J, Toader A, Munteanu C, Boyadjiev S, Madarász J, Pokol G, Zaharescu M (2016) J Therm Anal Calorim 124:71–80
32. Qu W, Jin W, Xu J, Yang S, Peng J (2012) Adv Mater Res 538-541:2438–2443
33. Znaidi L (2010) Mater Sci Eng B 174:18–30
34. Ghule AV, Ghule K, Chen C-Y, Chen W-Y, Tzing S-H, Chang H, Ling Y-C (2004) J Mass Spectrom 39:1202–1208
35. Corma A, Garcia H (2003) Chem Rev 103:4307–4365
36. Cesano F, Scarano D, Bertarione S, Bonino F, Damin A, Bordiga S, Prestipino C, Lamberti C, Zecchina A (2008) J Photochem Photobiol A: Chem 196:143–153
37. Kitano M, Arai K, Kodama A, Kousaka T, Nakajima K, Hayashi S, Hara M (2009) Catal Lett 131:242–249
38. Wang L, Mei T, Liu W, Zhou Q (2016) J Phys Chem C 120:5326–5330